Analysis of Energy Consumption Performance towards Optimal Radioplanning of Wireless Sensor Networks in Heterogeneous Indoor Environments

Peio LÓPEZ ITURRI[1], Leire AZPILICUETA[1], Juan Antonio NAZABAL[1],
Carlos FERNÁNDEZ-VALDIVIELSO[1], Jesús SORET[2], Francisco FALCONE[1]

[1] Dept. of Electrical and Electronic Engineering, Public Univ. of Navarre, Campus de Arrosadía, 31006, Pamplona, Spain
[2] Dept. of Electrical and Electronic Engineering, University of Valencia, Burjassot, Valencia, Spain

{peio.lopez, leyre.azpilicueta, juanantonio.nazabal, carlos.fernandez, francisco.falcone} @unavarra.es, jesus.soret@uv.es

Abstract. *In this paper the impact of complex indoor environment in the deployment and energy consumption of a wireless sensor network infrastructure is analyzed. The variable nature of the radio channel is analyzed by means of deterministic in-house 3D ray launching simulation of an indoor scenario, in which wireless sensors, based on an in-house CyFi implementation, typically used for environmental monitoring, are located. Received signal power and current consumption measurement results of the in-house designed wireless motes have been obtained, stating that adequate consideration of the network topology and morphology lead to optimal performance and power consumption reduction. The use of radioplanning techniques therefore aid in the deployment of more energy efficient elements, optimizing the overall performance of the variety of deployed wireless systems within the indoor scenario.*

Keywords

Radioplanning, wireless sensor networks, energy consumption, ray launching, CyFi.

1. Introduction

The use of wireless sensor networks is growing rapidly into a large number of fields of application, such as industrial monitoring, farming and agriculture, structural monitoring, health assistance, location and guiding or security and defense, among others [1-8]. The use of these wireless sensor networks within domestic environments is leading towards the fast paced development of the so called smart homes, linked with the more global concept of Internet of Things. One of the key issues is to reduce energy consumption of the individual elements of these wireless sensor networks, due to the fact that in the near future, a great deal of these devices will be operating within a conventional indoor environment. This is in line with ambitious energy reduction strategies, such as those stated in Europe 20/20 strategy.

Typically, the deployment of wireless systems is performed by initial coverage estimations (usually by empirical based models) which can later on be validated by field measurements. These field measurements, in the case of WLAN/WPAN systems are performed by using sniffers or protocol analyzers in order to obtain estimations of RSSI values and initial metrics of link level quality, such as Packet Error Ratio levels. In the case of mobile networks, performance analysis is conducted typically by means of test drives and Key Performance Indicator validation, based on mobile terminal tracing as well as by correlation to network statistics managed by the radio subsystem. Even though these approaches give an initial point to validate network operation, issues such as intra-system or inter-system interference are not considered, as well as the large variability in signal strength and quality due to the strong multipath characteristics inherent to indoor scenarios. Furthermore, not only coverage should be considered but also dynamic variation due to changes in traffic demands (and hence, in overall interference values) should be taken into account, leading to coverage-capacity relations. This is a relevant issue that is gaining importance as a larger amount of wireless networks are coexisting, leading to a heterogeneous wireless environment.

Moreover, minimizing energy consumption has become one of the main goals, driven by international Green policies. In this context, radio channel features of indoor environments pose a challenge to energy consumption, due to the fact that the complexity of the scenario increases losses due to strong multipath propagation and multi-screen diffraction, as well as absorption due to lossy dispersive media, as it is shown in previous works [9]. The existence of interference sources in these complex environments also affects the deployment strategies and overall power consumption [10].

In this paper, the topological influence of a layout of in-house developed CyFi based wireless sensors will be analyzed in terms of power consumption and radio coverage. For that purpose, the characteristics of the CyFi motes are presented in Section 2. Then, in Section 3, the analysis of the considered scenario by means of an in-house devel-

oped 3D ray tracing simulation tool is presented, showing radioplanning results as received power planes, power delay profiles or current consumption planes. Finally, in Section 4, received power and consumption measurements are presented for different test cases, showing the dependence between network topology and power consumption. In conclusion, the application of deterministic radioplanning approaches, like the method presented in this work, lead to an optimal network configuration, minimizing energy consumption and achieving desired quality of service.

2. CyFi Wireless Devices

For the purpose of this work, a system based on a set of wireless motes has been designed in house by the University of Valencia. Each mote includes sensor/actuator elements, a PSoC processor core, expansion ports and power, and a CyFi transceiver. Depending on the role that the nodes play in the protocol, the motes can be configured as a master or as a slave.

The basic network topology is a star configuration, in which a master node manages a certain number of peripheral slave nodes. Following a hierarchical scheme, different master nodes can be connected at slave-type stages to form a second layer around a master node that is responsible for monitoring the platform. Each mote has two parts: a main card which contains the microcontroller, and an additional one that contains the radio frequency part. The main board consists of different blocks, as shown schematically in Fig. 1. The real implementation can be seen in Fig. 2.
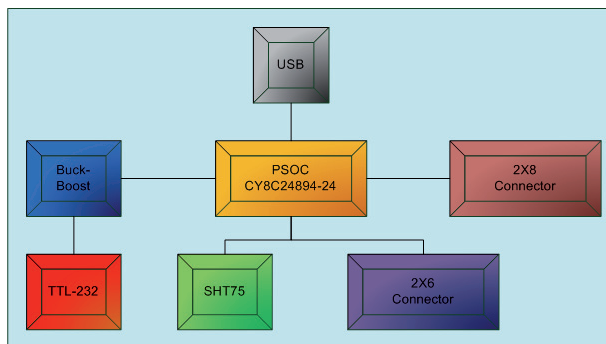

Fig. 1. Block diagram for the implemented mote device.

Fig. 2. Image of the main board (left) and the radio frequency module (right) of the mote device.

The microcontroller is the Cypress CY8C24894 PSoC. It incorporates an 8-bit microcontroller M8C and up to 4 MIPS. As reconfigurable elements, it contains 4 digital blocks and 6 analog blocks, in addition to 1KB of SRAM and 16KB of Flash. Also, the device has the possibility to communicate via USB without requiring any additional items. The humidity and temperature sensor used is an SHT75 model. This is calibrated at the factory, controlled digitally, has high resolution and accuracy, with an operating range of 0-100% relative humidity and a temperature range between -40ºC and 123ºC.

The used CyFi technology is a cost effective low-power wireless solution developed by Cypress Semiconductor that operates in the unlicensed 2.4 GHz ISM band, with active link and power management features. The network topology consists in a simple star network controlled by a central hub. Due to the lightweight network protocol stack of CyFi nodes, a bidirectional communication to up to 250 nodes is provided. CyFi output maximum power is 4 dBm and the receiver sensitivity -97 dBm, with a typical range in a line of sight, interference-free environment between 50 m and 70 m.

The mentioned active link and power management provide interesting dynamic functionalities. For more robustness, the transmitter changes the modulation and data rates dynamically between 1 Mbps and 250 Kbps depending on the environment's interference. If the interference increases, then the power output level is dynamically increased to overcome that interference. Besides, if a node detects that its power output is excessive, it will dynamically reduce it, reducing power consumption. Also, to ensure that the central hub of the network receives packets correctly, an interference free channel is selected whenever possible. If the hub detects a noisy channel, a CyFi network will look for a clean channel and settle there. The dynamic power handling capability, in terms of coverage/capacity estimation, will lead to smaller coverage radius as overall transmission speed increases, as will be shown in the following sections.

3. Indoor Scenario Analysis

In order to perform estimations of the influence of the indoor environment in a wireless sensor network, radioplanning simulation results have been obtained. For that purpose, radiopropagation analysis can be performed by means of empirical methods (such as COST-231, Walfish-Bertoni, Okumura Hata, etc.) [11-13], based on statistical approaches and non-linear regression techniques. They give rapid results but require calibration based on measurements to give an adequate fit of the results. On the other hand, deterministic methods [14-20] are based on numerical approaches to the resolution of Maxwell's equations, such as ray launching and ray tracing (based on geometrical approximations) or full-wave simulation techniques (method of moment (MoM), finite difference time domain (FDTD) [21], FITD, etc.). These methods are precise but are time-consuming to inherent computational complexity.

As a midpoint, methods based on geometrical optics, for radioplanning calculations with strong diffractive elements, offer a reasonable trade-off between precision and required calculation time [22]. The Ray Tracing method combined with uniform theory of diffraction (UTD) [23] is most frequently applied to radio coverage prediction [24-27]. The Ray Tracing models, including modifications as reception sphere technique [28], potentially represent the most accurate and versatile methods for urban and indoor multipath propagation characterization or prediction [29-33].

3.1 Simulation Technique

This work presents an in-house developed 3D Ray Launching algorithm to analyze the influence of the indoor environment in the propagation of electromagnetic signals, validated in previous works [34-38]. The novelty of the proposed method is that it takes into account all the obstacles within the scenario, with their different shapes and material properties. It is important to emphasize that a grid is defined in the space to save the parameters of each ray. Accordingly, the environment is divided into a number of cuboids of a fixed size. When a ray enters a specific hexahedron, its parameters are saved in a matrix. Electromagnetic phenomena such as reflection, refraction and diffraction are taken into account, based on Geometrical Optics and Geometrical Theory of Diffraction. Firstly, an indoor scenario has been created, taking into account the material parameters of all of the elements within it (e.g., furniture, walls, windows, etc.), in terms of conductivity and dielectric permittivity. Electromagnetic phenomena such as reflection, refraction and diffraction have been taken into consideration.
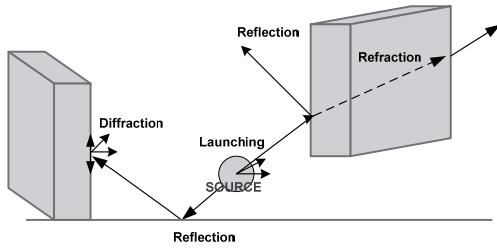

Fig. 3. Principle of Ray Launching method.

Fig. 3 shows the principle of ray launching method. The equivalent transmitter antenna located in the simulation scenario launches rays in different directions following the radiation pattern of the antenna. The reflection and refraction coefficients are calculated using the well-known Fresnel's equations by

$$T^{\perp} = \frac{E_t^{\perp}}{E_i^{\perp}} = \frac{2\eta_2 \cos(\Psi_i)}{\eta_2 \cos(\Psi_i) + \eta_1 \cos(\Psi_t)} ,\tag{1}$$

$$R^{\perp} = \frac{E_r^{\perp}}{E_i^{\perp}} = \frac{\eta_2 \cos(\Psi_i) - \eta_1 \cos(\Psi_t)}{\eta_2 \cos(\Psi_i) + \eta_1 \cos(\Psi_t)} ,\tag{2}$$

$$R^{\parallel} = \frac{E_r^{\parallel}}{E_i^{\parallel}} = \frac{\eta_1 \cos(\Psi_i) - \eta_2 \cos(\Psi_t)}{\eta_1 \cos(\Psi_i) + \eta_2 \cos(\Psi_t)} ,\tag{3}$$

$$T^{\parallel} = \frac{E_t^{\parallel}}{E_i^{\parallel}} = \frac{2\eta_2 \cos(\Psi_i)}{\eta_1 \cos(\Psi_i) + \eta_2 \cos(\Psi_t)}\tag{4}$$

where $\eta_1 = 120\pi / \sqrt{\varepsilon_{r1}}$, $\eta_2 = 120\pi / \sqrt{\varepsilon_{r2}}$ and Ψ_i, Ψ_r, Ψ_t are the incident, reflected and transmitted angles respectively.

The diffraction coefficients are considered by the Uniform Theory of Diffraction (UTD) [39-40] as follows

$$D^{\parallel\perp} = \frac{-e^{(-j\pi/4)}}{2n\sqrt{2\pi k}} \left\{ \begin{array}{l} \cot\left(\frac{\pi + (\Phi_2 - \Phi_1)}{2n}\right) F\left(kLa^+(\Phi_2 - \Phi_1)\right) \\ + \cot\left(\frac{\pi - (\Phi_2 - \Phi_1)}{2n}\right) F\left(kLa^-(\Phi_2 - \Phi_1)\right) \\ + R_0^{\parallel\perp}\cot\left(\frac{\pi - (\Phi_2 + \Phi_1)}{2n}\right) F\left(kLa^-(\Phi_2 + \Phi_1)\right) \\ + R_n^{\parallel\perp}\cot\left(\frac{\pi + (\Phi_2 + \Phi_1)}{2n}\right) F\left(kLa^+(\Phi_2 + \Phi_1)\right) \end{array} \right\}$$

$$\tag{5}$$

where $n\pi$ is the wedge angle, Φ_2 and Φ_1 angles, F, L and $a\pm$ are defined in [39], $R_{0,n}$ are the reflection coefficients for the appropriate polarization for the 0 face or n face, respectively.

The commitment between accuracy and computational time is acquired with the number of launching rays and the cuboids size of the considered scenario. Several transmitters can be placed within an indoor scenario. Parameters such as frequency of operation, radiation patterns of the antennas, number of multipath reflections, separation angle between rays and cuboids dimension are introduced. Fig. 4 depicts ray launching method within a defined indoor scenario.
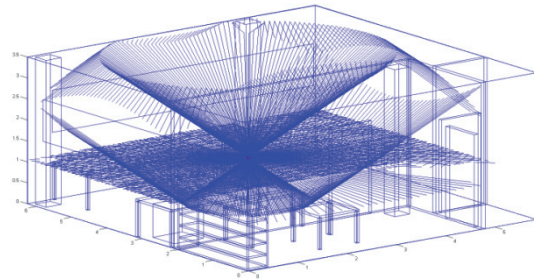

Fig. 4. Schematic of 3D ray launching within an indoor scenario.

The scenario that has been analyzed in this paper is the Radiocommunication Laboratory, placed in the Electric and Electronic Engineering Department of the Public University of Navarra. The scenario has the inherent complexity of an indoor scenario, as it has interior columns, many furniture elements, different types of instruments and walls made of different materials (wood, concrete, bricks, metal and glass). The scenario can be seen in Fig. 5a and its schematic representation for the ray launching software can be seen in Fig. 5b. Red points in Fig. 5b represent the different points where the wireless motes have been placed. These positions have been chosen in order to simulate a possible morphology of a real wireless network. For that

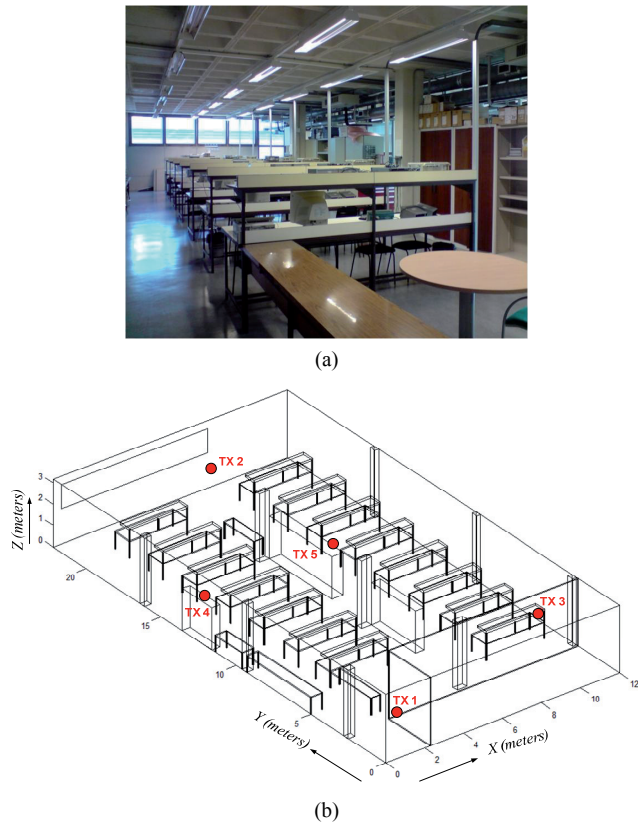reason, the motes have been placed at different heights. The exact coordinates for the motes are shown in Tab. 1.

(a)

(b)

Fig. 5. (a) Indoor scenario under analysis, corresponding to Radiocommunication Laboratory, UPNA. (b) Schematic description of the scenario in the 3D ray launching software.

Transmitter	Coordinates
TX1	(2, 2, 0.81) m
TX2	(6.5, 21, 2.7) m
TX3	(11, 4, 1.5) m
TX4	(0.3, 12.5, 2.1) m
TX5	(7, 12.5, 2.1) m

Tab. 1. Coordinates where the wireless motes are placed in the indoor scenario.

3.2 Simulation Results

3D ray launching simulation results have been obtained for the whole volume of the simulation scenario. The parameters used in the simulation are the following: uniform cuboids resolution of 20 cm, vertical plane angle resolution $\Delta\theta = \pi/180$, horizontal plane angle resolution $\Delta\Phi = \pi/180$, maximum number of tolerated reflections $N = 5$, frequency of operation 2.4 GHz and power transmission of 4 dBm. The considered parameters are equivalent to those of a conventional ZigBee system. Fig. 6 shows the obtained received power levels for the same bidimensional plane at height 0.81 m (the same height as the tables within the laboratory) for different number of transmitters. For each of the represented planes (from Fig. 6a to Fig. 6e), a new transmitter has been added consecutively, starting

with a single transmitter (Fig. 6a) and finishing with a wireless network composed by five transmitters (Fig. 6e).
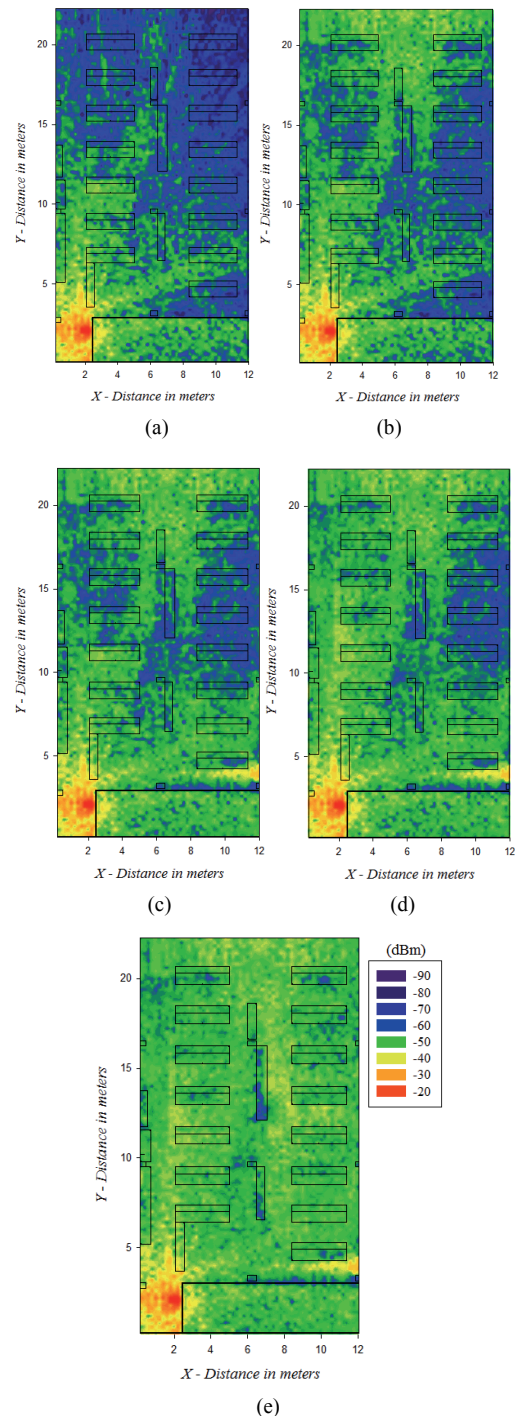

(a)

(b)

(c)

(d)

(e)

Fig. 6. RSSI 3D ray launching simulation results obtained at a bidimensional plane at a height of 0.81 m for different number of transmitters: (a) TX 1, (b) TX1 and TX2, (c) TX1, TX2 and TX 3, (d) TX1, TX2, TX3 and TX4, (e) TX1, TX2, TX3, TX4 and TX5.

As it can be seen from the previous figures, received power level is strongly dependent on the position of the potential receiver element and the morphology of the wireless network. Variations can be in order of 10 dB within 1 meter when the number of transmitters is low,

which has a strong impact on the performance of the sensors, not only in terms of receiver sensitivity limits but also on overall system capacity, which is dependent on signal level as well as on signal to noise ratio. As it is shown in Fig. 6, this received power variations can be strongly mitigated changing the morphology (e.g. adding wireless motes) of the wireless network, thus obtaining a reasonable received power level for every position of the complete indoor scenario.

The multipath propagation is the strongest phenomenon in this type of complex indoor environments, hence, to appreciate the variability of estimated received power level more precisely, Fig. 7 shows this variability within a given line path for a fixed value of X for two different heights in the indoor scenario. The X value has been set to 3.5 m randomly, since this phenomenon happens all alike within the whole scenario. As stated above, the signal variation is driven by strong multipath components, as can be seen from the short term variation component within the received power level. For a more thorough analysis of the impact of the multipath propagation in the scenario, time domain results are shown in Fig. 8 and Fig. 9. Specifically, power delay profiles are presented for the locations of TX2 and TX3 respectively, when TX1 transmits. A red line has been depicted in both graphics to delimit the sensitivity level of the CyFi motes. As expected, a lot of components reached the TX2 and TX3 points due to the multipath propagation, but in Fig. 8, which corresponds to the farthest mode of the network (from TX1), there are a lot of components under the sensitivity level, due mainly the distance. On the other hand, in Fig. 9 most of the components are above the sensitivity level, as it corresponds to the nearest node of the network. In order to complete the time domain results, the delay spread for a plane of 0.81 m height (the height of the tables and TX1) is presented in Fig. 10.
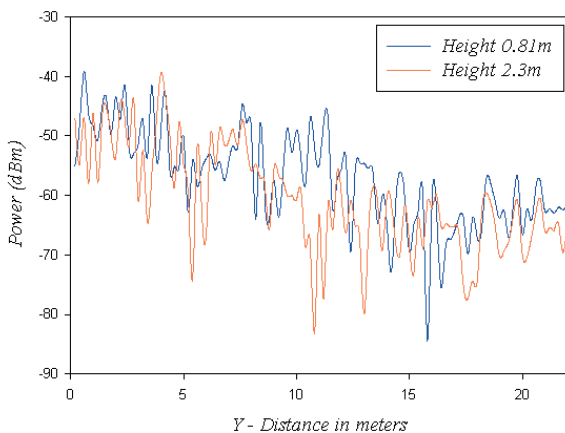

Fig. 7. Simulation results for height 0.81 m and height 2.3 m, for X = 3.5 m, along the Y-axis of the indoor scenario under analysis.

The obtained simulation results and mainly the estimated values of received power can lead to the analysis of the performance of the wireless system. As an example, Fig. 12 represents the signal to noise ratio (SNR) for two different heights in the same scenario, which could be used to consider the most adequate deployment strategy of a set
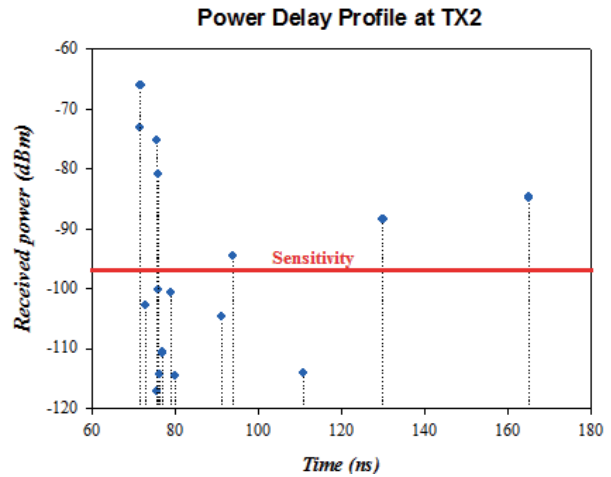

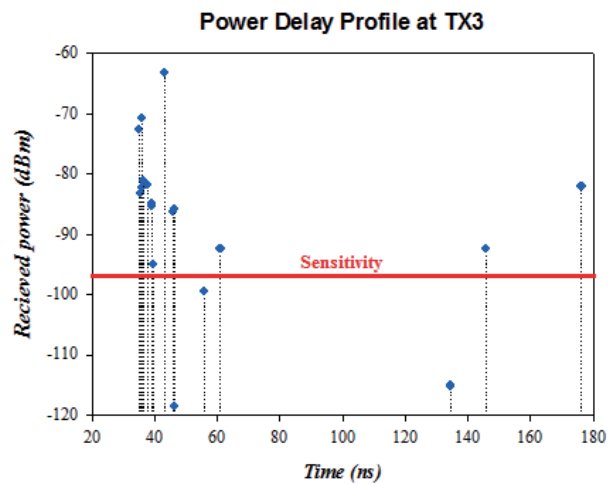**Fig. 8.** Power Delay Profile at location of TX2 (the farthest node), while TX1 is transmitting.

Fig. 9. Power Delay Profile at location of TX3 (the nearest node), while TX1 is transmitting.
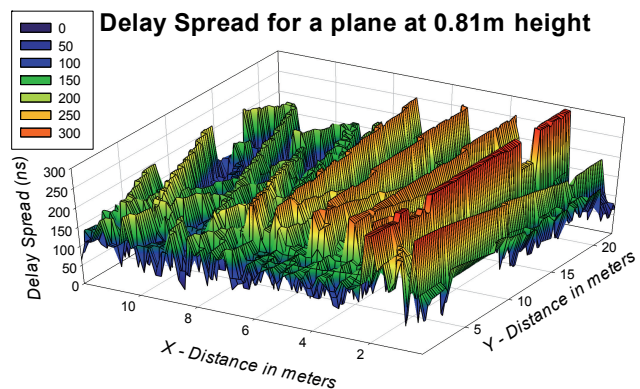

Fig. 10. Delay Spread values for a plane at 0.81 meters height (i.e. the height of TX1 within the scenario).

of wireless sensor networks within the indoor scenario. Specifically, SNR planes depicted in Fig. 12 have been calculated taking into account that the whole CyFi network is deployed (see Fig. 6e) and as noise sources, an interfering WiFi network (an access point and 3 laptops) operating at the same frequency band of the CyFi motes has been simulated. The simulation parameters have been the same

than those used for the simulation of the CyFi motes, but the transmitted power of WiFi nodes has been set to 20 dBm, which corresponds to a typical maximum transmitted power of a commercial device. In Fig. 11 the schematic configuration of the wireless networks within the scenario is shown. Tab. 2 shows the position within the scenario of the WiFi nodes.

Device	Coordinates
WiFi access point	(3, 3, 2.5) m
Laptop1	(4.5, 6.9, 0.9) m
Laptop2	(2, 13.5, 0.9) m
Laptop3	(8.5, 17.7, 0.9) m

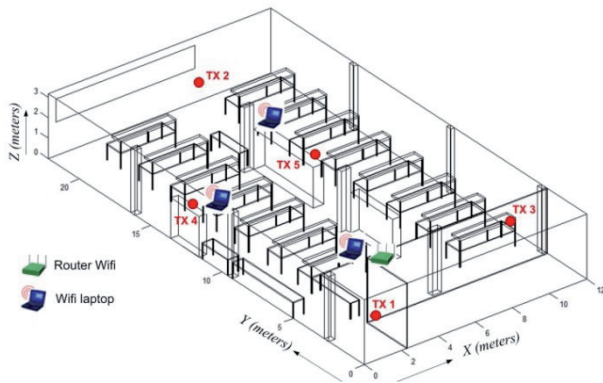**Tab. 2.** Coordinates where WiFi devices have been placed within the scenario.

Fig. 11. Schematic representation of the scenario used to calculate the SNR planes of Fig. 12.
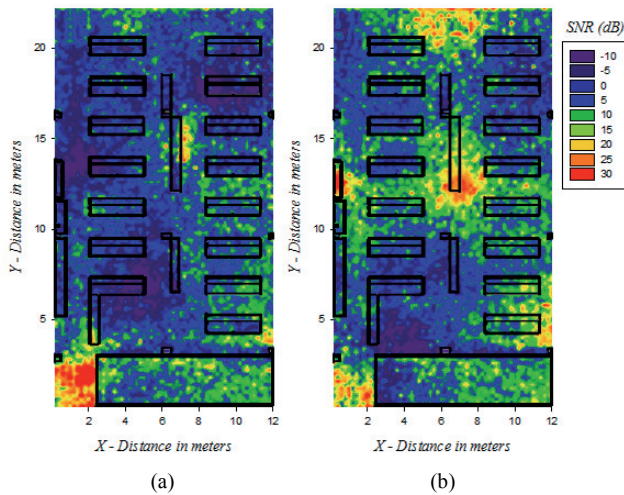

Fig. 12. Spatial distribution of signal to noise ratio in the indoor scenario of Fig. 5 for two different heights: (a) 0.81 meters, (b) 2.3 meters.

Thus, the SNR value is obtained for each point within the room, giving valuable information about the zones and points where the placement of a mote will be better in terms of received signal quality, whilst maintaining the optimal wireless power transmission (and hence energy consumption) of the system. As can be clearly seen in Fig. 12, the zones where interfering devices have been placed are the zones with lower SNR, as expected. For a more in-depth analysis of the proposed CyFi network in

terms of SNR, in Fig. 13, the SNR at each receiver CyFi mote is depicted, when a single mote is transmitting. In Tab. 3 the preset transmission power levels for the CyFi motes are shown, which have been used for the calculation of the SNR, in order to show how it affects the SNR at the receiver motes. As the CyFi motes can change dynamically the transmission rate between 1 Mbps and 250 Kbps, the minimum SNR needed has been calculated for both data rates, and these limits have been depicted by red dashed lines (0 dB for 1 Mbps, and -7.23 dB for 250 Kbps). Fig. 13a shows the results for the worst noise case, i.e. when the WiFi devices transmit 20 dBm, whilst Fig. 13b shows the results for WiFi devices transmitting 0 dBm. These results show that the presented method can aid in an adequate deployment strategy within a harsh indoor scenario, which has a direct impact on the network efficiency.

Defined internal level	Transmitted power (dBm)
7	4
6	0
5	-5
4	-13
3	-18
2	-24
1	-30
0	-35

Tab. 3. CyFi motes' preset levels and their correspondent transmission power level.
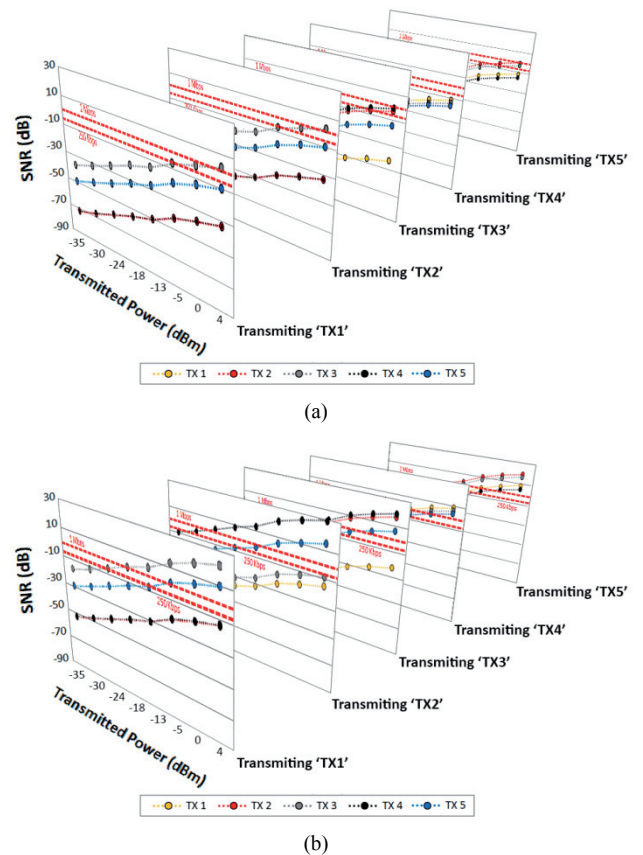

(a)

(b)

Fig. 13. SNR values at each CyFi mote position for a single transmitting mote, while WiFi-interference sources are transmitting (a) 20 dBm and (b) 0 dBm.

Considering the overall power consumption of the deployed motes is also a highly important issue in radio planning strategies. As it has been shown previously, the location of the transceiver has a significant role in terms of the variations of the expected value of received power within the scenario, which has a great impact on the power consumption of transmitting motes. This is given by the fact that as the received power varies, the link balance within the sensitivity threshold limit also varies, modifying the required current for the transceiver to operate. Therefore, it is possible to estimate energy consumption of the transmitter as a function of the receiver location. In order to gain insight on the effect of topology and morphology on energy consumption in the previous scenario, Fig. 14 shows the consumption increase maps for two cases: first when only two motes are operating (TX1 and TX2) and afterwards when the whole wireless network is operating (5 transmitters), which corresponds to the optimal configuration of the network for the presented indoor scenario.
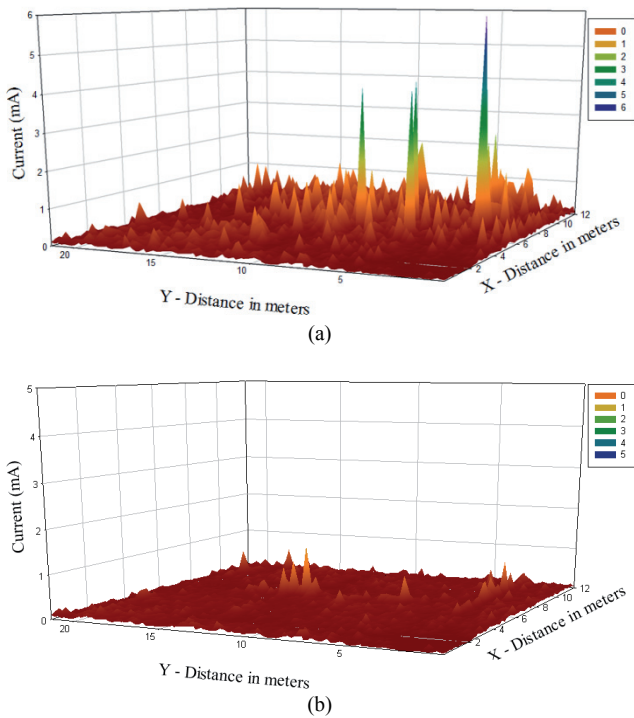

(a)

(b)

Fig. 14. Estimation of energy consumption in terms of current values in mA for different locations of the scenario depicted in Fig. 5.

These maps represent the overall increase of current consumption of the transmitting motes placed at the scenario for each possible receiver location. From the real measurements explained in the next section, it is shown that the lowest measured consumption of a mote when transmitting is 40.5 mA (distance between transmitter and receiver of 5 cm). So, as it can be seen in the consumption maps for the first case (Fig. 14a), a maximum current consumption increase of 6.03 mA is reached for a specific location (this maximum peak seems not to reach that value, but it is due to the perspective of the graph). This corresponds to the worst location for a receiver to be placed in terms of current consumption. This means that for that receiver loca-

tion, the overall current consumption for the transmitters will increase in 6.03 mA due to the power level received at that location, which is equal to 14.8% more consumption. On the other hand, for the optimal case of 5 transmitters deployed (Fig. 14b), the worst receiver location implies an increase of 3.11% of the total consumption of the five transmitting motes of the network. This lower increase of consumption is expected as the received power level for the whole scenario is higher due to the higher amount of deployed transmitting nodes.

These results can be really useful in order to plan the design of the optimal network, taking into account the number of employed nodes, the required transmission bandwidth and the sensitivity level. Moreover, as it is shown in Fig. 14, the density of the nodes within the network has a clear impact on energy consumption, due to the fact that link balance limitations are lower when the whole network is operating. Nevertheless, it is important to achieve a commitment between the density of nodes and interference levels, because a larger number of nodes could lead to increased interference levels, which could degrade system performance.

4. Measurement Results of Deployed Wireless Sensors

In order to validate the previously obtained simulation estimations, in which the morphological dependence of the network performance in terms of received signal is observed, wireless CyFi motes have been configured and measured. For that purpose, power distribution and current consumption measurement results are presented. In Fig. 15, a layout of the tested setup is shown. The laboratory has two zones, separated by several metallic shelves. For the purpose of the study, the left hand zone has been measured, due to the fact that this is a zone of interaction with students and collaborators, leading to a realistic situation for the deployment and use of a wireless sensor network. The measurements have been performed by programming a test setup among the motes, given by a coordinator element and a wireless sensor.
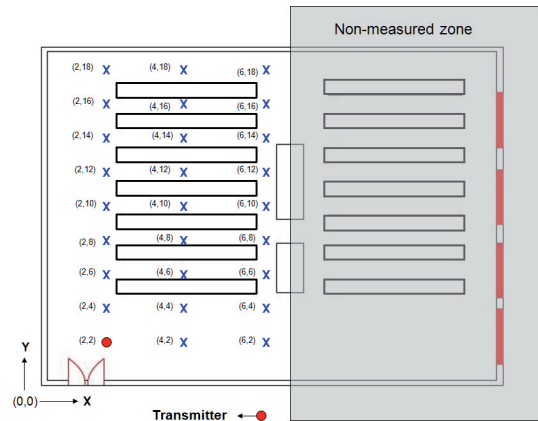

Fig. 15. Schematic of the indoor scenario (Public University of Navarre).

Initially, the RSSI values in different points of the scenario (Fig. 15) have been measured: The transmitter is located in coordinates (2, 2) and it is represented by a red point. The receiver has been placed in different points, which are represented by blue X marks in the figure. Both the transmitter and receiver have been placed at the same height of 81 cm, which is the height of the tables located in the scenario. The same antenna orientation in all the measurements has been carefully maintained in order to minimize variations due to the radiation pattern of the receiving antenna. The motes have been programmed to transmit at low data rate of 1 packet every 20 seconds, emulating a possible wireless sensor network application linked to Ambient Intelligence or Smart Homes. The RSSI values have been read directly from the data provided by the motes, by means of protocol analysis of the air interface. The obtained values for different positions in the laboratory are shown in Fig. 16. The scale has been set up to -100 dBm in order to account for the sensitivity value of the motes (-97 dBm). As expected, due to the CyFi's active link and power management, signal level does not clearly decrease with the distance as it happens in a common radiowave transmission (with a transmitter transmitting a fixed power level). The signal level is maintained quite well within the scenario, although variations on received power can be seen due to the multipath radiopropagation effects (mainly diffraction and reflection), very significant in an indoor complex scenario like this.
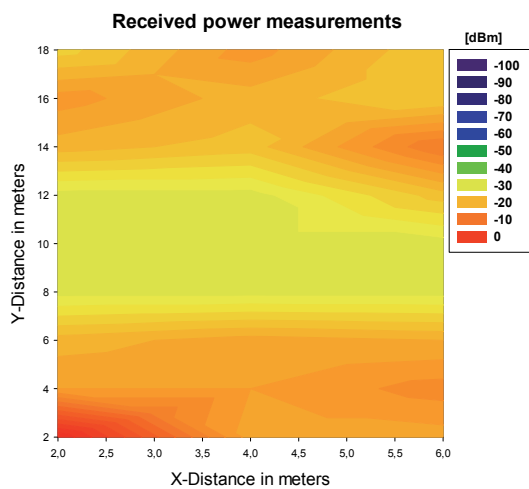

Fig. 16. Measured power levels in dBm for a pair of mote coordinator/sensor in the indoor scenario.

To gain more insight in the operation of the sensor motes and the influence of the topology and morphology of the scenario, current consumption has been measured for several positions. For that purpose, the motes have been programmed to transmit at their highest packet transmission rate (1 packet per 15 ms) and the highest transmission power level (4 dBm) in order to increase the current demand of the motes. As in the previous case, both the transmitter and receiver have been placed at the same height of 81 cm. With this new approach, unlike the previous case, at certain distance from the coordinator no packets are received. The RSSI values shown in Fig. 17 are the mean values of the RSSI data of the packets received in a 2-second duration time slot, which correspond approximately to 130 packets as long as the communication has been correctly done.
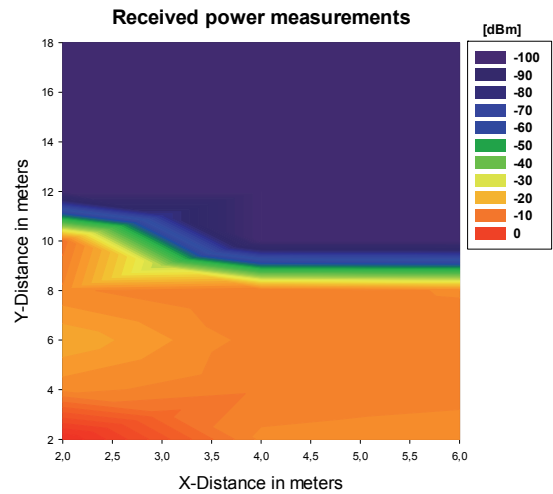

Fig. 17. Measured power levels in dBm for a pair of mote coordinator/sensor in the indoor scenario at highest transmission data rate.

When the distance is higher, the communication has problems and the number of received packets decreases up to 10 packets in 2 seconds due to the approach of the received power to the sensitivity level of the motes. Fig. 17 shows how the received power level near the transmitter is quite constant as well as the sensitivity level zone, in which no packets are received. This is due, once again, to the automatic regulation of transmit power that is embedded in the motes. But, despite of that, variations on received power level could be measured (on a smaller extent than in a case without transmitter power regulation), once again, due to the particularities of radiopropagation within a heterogeneous scenario with a complex morphology like this (a lot of furniture composed of different materials). As an example, although coordinates (6,6) are located further from the transmitter than coordinates (2,6), and the transmitter tries to maintain the received power level throughout the scenario, the zone corresponding to coordinates (2,6) has lower received power level. It is worth noting that due to the increase in the overall transmission rate, the sensitivity of the motes is decreased, leading to lower coverage zones, as clearly observable from Fig. 17. This again is given by the auto regulation power function embedded within the motes, reducing the available transmission power in order to handle a decreased sensitivity value given by a higher transmission speed. As an example, a PER (Packet Error Rate) measurement has been made between a transmitter in (2,2) and a receiver in (2,6). As mentioned previously, a low received power zone is detected surrounding the coordinate (2,6). This zone has the same characteristics as the zone near the sensitivity level, in which the number of received packets decreases abruptly. This is clearly shown in the PER value obtained for the transmission of 100,000 packets: only 1,363 packets arrived (PER = 98.637 %).

In order to see the evolution of the current consumption of the transmitter in this scenario, the receiver has been placed at different distances from the transmitter. A Tektronix DPO 3014 oscilloscope has been used to obtain the current consumption measurements. For this purpose, a 1 ohm resistor has been introduced in series in the feeding circuit of the mote. In this way, by measurement of the voltage difference in the resistor, an estimation of the current value is obtained. The obtained results are shown in Fig. 18 and Fig. 19.
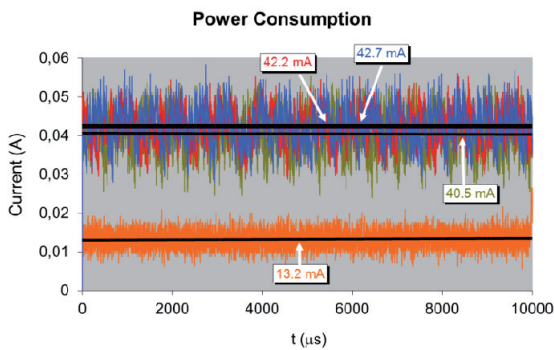

Fig. 18. Power consumption variation as a function of time for different positions. The bottom curve (13.2 mA) is for standby, whereas as the rest of the curves span from the closest to the farthest mote within the measurement scenario.
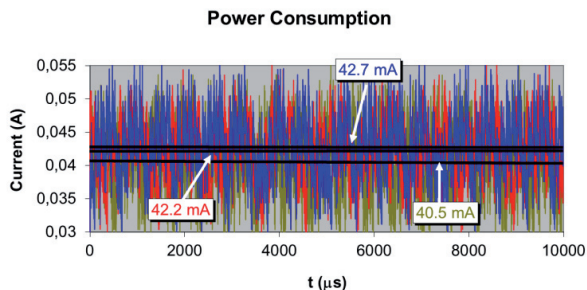

Fig. 19. Detail on the power consumption for the designed mote device within the indoor scenario. The mean values for different currents are proportional to the separation between motes.

As it can be seen in Fig. 18, a clear difference exists between the standby (orange curve) and the transmit mode (the rest of the curves), which is expected due to the normal operational procedure in the wireless transceiver. In Fig. 19, a detail of the different transmit mode current values can be seen, given for different positions of the sensor within the scenario. These distances have been 0.05 m, 2 m and 4.2 m, respectively. The last distance corresponds to the point in which the sensitivity level has been almost reached, in which few packets are received. This sensitivity point varies between 4 and 6 m depending on the environment and the objects surrounding the motes. From the measured values of the current consumption from the motes in operating mode at different distances, an increase in current consumption in the order of 4.2% in the case of 2 m and 5.4% in the case of 4.2 m is observed. Therefore, by considering the pre-existent levels of inter-ference as well as the expected fading losses of the scenario, the optimal location of the motes can be planned prior to real network deployment.

As the distance increases, the power consumption level also increases, which is in accordance to the operation of the power management of CyFi motes: By increasing the distance between motes, the receiver power decreases. But due to the power management features of the motes, the transmitted power level increases in order to maintain the received power level in each position, leading to higher power demands of the transmitter.

5. Conclusions

In this work, the topological and morphological influence in the operation of a wireless sensor network is described. An indoor scenario has been analyzed by means of deterministic 3D ray launching in-house algorithm as well as by measurements with an in-house developed wireless sensor platform. The results show that the radiopropagation characteristic of indoor scenarios is complex, leading to strong topological dependences in the overall received signal power, which affects other parameters such as capacity of the wireless sensor network. The results show that by considering radioplanning issues in the deployment of the wireless sensor networks, power consumption as well overall system performance can be strongly optimized, due to direct impact on energy consumption of the wireless transceivers. In the future, these results can aid deployment and planning of complex indoor sensor networks, optimizing the overall power consumption without degrading system performance. With the advent of LTE and Internet of Things, the use of precise radioplanning techniques to aid in wireless transceiver deployment can be a determining factor for successful adoption of these emerging technologies.

Acknowledgements

References

[1] BOSE, R. Sensor networks-motes, smart spaces and beyond. *IEEE Pervasive Computing*, 2009, vol. 8, no. 3, p. 84–90.

[2] GROSSE, C.U., GLASER, S.D., KNUGER, M. Initial development of wireless acoustic emission sensor motes for civil infrastructure state monitoring. *Smart Structures and Systems*, 2010, vol. 6, no. 3, p. 197–209.

[3] BUCKNER, B.D., MARKOV, V., LAI, L.C., EARTHMAN, J.C. Laser-scanning structural health monitoring with wireless sensor motes. *Optical Engineering*, 2008, vol. 47, no. 5, Art. No. 054402.

[4] BERISHA, V., KWON, H., SPANIAS, A. Real-time acoustic monitoring using wireless sensor motes. In *Proceedings of the IEEE International Symposium on Circuits and Systems*. Island of Kos (Greece), 2006, p. 847–850.

[5] TRUBILOWICZ, J., CAI, K., WEILER, M. Viability of motes for hydrological measurements. *Water Resources Research*, 2009, vol. 45, Art. No. W00D22.

[6] KUANG, K.S.C., QUEK, S.T., MAALEJ, M. Remote flood monitoring system based on plastic optical fibers and wireless motes. *Sensors and Actuators A – Physical*, 2008, vol. 147, no. 2, p. 449–455.

[7] YUNSEOP, K., EVANS, R.G., IVERSEN, W.M., Remote sensing and control of an irrigation system using a distributed wireless sensor network. *IEEE Transactions on Instrumentation and Measurement*, 2008, vol. 57, no. 7, p. 1379–1387.

[8] RUIZ-GARCÍA, L., BARREIRO, P., ROBLA, J.I., LUNADEI, L. Testing ZigBee motes for monitoring refrigerated vegetable transportation under real conditions. *Sensors*, 2010, vol. 10, no. 5, p. 4968–4982.

[9] NAZABAL, J.A., LOPEZ ITURRI, P., AZPILICUETA, L., FALCONE, F., FERNÁNDEZ-VALDIVIELSO, C. Performance analysis of IEEE 802.15.4 compliant wireless devices for heterogeneous indoor home automation environments. *International Journal of Antennas and Propagation*, 2012, article number 176383.

[10] LOPEZ ITURRI, P., NAZABAL, J.A., AZPILICUETA, L., RODRIGUEZ, P., BERUETE, M., FERNÁNDEZ-VALDIVIELSO, C., FALCONE, F. Impact of high power interference sources in planning and deployment of wireless sensor networks and devices in the 2.4 GHz frequency band in heterogeneous environments. *Sensors*, 2012, vol. 12, no. 11, p. 15689–15708.

[11] HATA, M. Empirical formula for propagation loss in land mobile radio services. *IEEE Transactions on Antennas and Propagation*, 1980, vol. 29, no. 3, p. 317–325.

[12] IKEGAMI, F., YOSHIDA, S., TAKEUCHI, T., UMEHIRA, M. Propagation factors controlling mean field strength on urban streets. *IEEE Transactions on Antennas and Propagation*, 1984, vol. 32, no. 8, p. 822–829.

[13] PHAIBOON, S., PHOKHARATKUL, P. Path loss prediction for low-rise buildings with image classification on 2-D aerial photographs. *Progress in Electromagnetics Research*, 2009, vol. 95, p. 135–152.

[14] LEE, S. H. A photon modeling method for the characterization of indoor optical wireless communication. *Progress in Electromagnetics Research*, 2009, vol. 92, p. 121–136.

[15] LEE, D. J. Y., LEE, W. C. Y. Propagation prediction in and through buildings. *IEEE Transactions on Vehicular Technology*, 2000, vol. 49, no. 5, p. 1529–1533.

[16] TAN, S. Y., TAN, H. S. A microcellular communications propagation model based on the uniform theory of diffraction and multiple image theory. *IEEE Transactions on Antennas and Propagation*, 1996, vol. 44, no. 10, p. 1317–1326.

[17] KANATAS, A. G., KOUNTOURIS, I. D., KOSTARAS, G. B., CONSTANTINOU, P. A UTD propagation model in urban microcellular environments. *IEEE Transactions on Vehicular Technology*, 1997, vol. 46, no. 1, p. 185–193.

[18] DIMITRIOU, A. G., SERGIADIS, G. D. Architectural features and urban propagation. *IEEE Transactions on Antennas and Propagation*, 2006, vol. 54, no. 3, p. 774–784.

[19] FRANCESCHETTI, M., BRUCK, J., SCHULMAN, L. J. A random walk model of wave propagation. *IEEE Transactions on Antennas and Propagation*, 2004, vol. 52, no. 5, p. 1304–1317.

[20] BLAS PRIETO, J.,LORENZO TOLEDO, R. M., FERNÁNDEZ REGUERO, P., ABRIL, E. J., BAHILLO MARTÍNEZ, A., MAZUELAS FRANCO, S., BULLIDO, D. A new metric to analyze propagation models. *Progress In Electromagnetics Research*, 2009, vol. 91, p. 101–121.

[21] SCHUSTER, J. W., LUEBBERS, R. J. Comparison of GTD and FDTD predictions for UHF radio wave propagation in a simple outdoor urban environment. In *IEEE Antennas and Propagation Society International Symposium*. 1997, vol. 3, p. 2022–2025.

[22] ISKANDER, M. F., YUN, Z. Propagation prediction models for wireless communications systems. *IEEE Transactions on Microwave Theory and Techniques*, 2002, vol. 50, p. 662–673.

[23] KOUYOUMJIAN, R. G., PATHAK, P. H. A uniform theory of diffraction for an edge in a perfectly conducting surface. *Proc. IEEE*, 1974, vol. 62, no. 4, p. 1448–1462.

[24] GENNARELLI, G., RICCIO, G. A UAPO-based model for propagation prediction in microcellular environments. *Progress in Electromagnetics Research*, 2009, vol. 17, p. 101–116.

[25] SON, H. W., MYUNG, N. H. A deterministic ray tube method for microcellular wave propagation prediction model. IEEE *Transact. on Antennas and Propagation*, 1999, vol. 47, no. 8, p. 1344–1350.

[26] TAYEBI, A., GÓMEZ J., DE ADANA, F. S., GUTIERREZ, O. The application of arrival and received signal strength in multipath indoor environments. *Progress In Electromagnetics Research*, 2009, vol. 91, p. 1–15.

[27] SONG, H. B., WANG, H. G., HONG, K., WANG, L. A novel source localization scheme based on unitary esprit and city electronic maps in urban environments. *Progress In Electromagnetics Research*, 2009, vol. 94, p. 243–262.

[28] LU, W., CHAN, K. T. Advanced 3D ray tracing method for indoor propagation prediction. *Electronics Letters,* 1998, vol. 54, no. 12, p. 1259–1260.

[29] SEIDEL, S. Y., RAPPAPORT, T. S. Site-specific propagation prediction for wireless in-building personal communication system design. *IEEE Transactions on Vehicular Technology*, 1994, vol. 43,no. 4, p. 879–891.

[30] DURGIN, G., PATWARI, N., RAPPAPORT, T. S. An advanced 3D ray launching method for wireless propagation prediction. In *IEEE 47th Vehicular Technology Conference*. Phoenix (AZ, USA), 4-7 May 1997.

[31] CHANG-FA YANG, BOAU-CHENG WU, CHUEN-JYI KO. A ray-tracing method for modeling indoor wave propagation and penetration. *IEEE Transactions on Antennas and Propagation*, 1998, vol. 46, no. 6, p. 907–919.

[32] LOTT, M. On the performance of an advanced 3D ray tracing method. In *Proc. of European Wireless & ITG Mobile Communication*. Munich (Germany), 6-8 Oct. 1999.

[33] ROSSI, J.-P., GABILLET, Y. A mixed ray launching/tracing method for full 3-D UHF propagation modeling and comparison with wide-band measurements. *IEEE Transactions on Antennas and Propagation*, 2002, vol. 50, no. 4, p. 517–523.

[34] AZPILICUETA, L., FALCONE, F., ASTRÁIN, J. J., VILLADANGOS, J., GARCÍA ZUAZOLA, I. J., LANDALUCE, H., ANGULO, I., PERALLOS, A. Measurement and modeling of a UHF-RFID system in a metallic closed vehicle. *Microwave and Optical Technology Letters*, 2012, vol. 54, no. 9, p. 2126–2130.

[35] AGUIRRE, E., ARPÓN, J., DE MIGUEL, S., RAMOS, V., FALCONE, F. Evaluation of electromagnetic dosimetry of wireless systems in complex indoor scenarios with human body interaction. *Progress In Electromagnetic Research B*, 2012, vol. 43, p. 189 to 209.

[36] LED, S., AZPILICUETA, L., AGUIRRE, E., MARTÍNEZ DE ESPRONCEDA, M., SERRANO, L., FALCONE, F. Analysis and description of HOLTIN service provision for AECG monitoring in complex indoor environments. *Sensors,* 2013, vol. 13, no. 4, p. 4947–4960.

[37] AGUIRRE, E., ARPON, J., AZPILICUETA, L., LOPEZ, P., DE MIGUEL, S., RAMOS, V., FALCONE, F. Estimation of electromagnetic dosimetric values from non-ionizing radiofrequency fields in an indoor commercial airplane environment. *Electromagnetic Biology and Medicine*, published online in Aug. 2013.

[38] AGUIRRE, E., LOPEZ ITURRI, P., AZPILICUETA, L., DE MIGUEL-BILBAO, S., RAMOS, V., GARATE, U., FALCONE, F. Analysis of estimation of electromagnetic dosimetric values from non-ionizing radiofrequency fields in conventional road vehicle environments. *Electromagnetic Biology and Medicine*, published online in Jan. 2014.

[39] LUEBBERS, J. R. A heuristic UTD slope diffraction coefficient for rough lossy wedges. *IEEE Transactions on Antennas and Propagation*, 1989, vol. 37, no. 2, p. 206–211.

[40] LUEBBERS, J. R. Comparison of lossy wedge diffraction coefficients with application to mixed path propagation loss prediction. *IEEE Transactions on Antennas and Propagation*, 1988, vol. 36, no. 7, p. 1031–1034.

About Authors …

Peio LÓPEZ ITURRI received his Telecommunications Engineering Degree from the Public University of Navarre (UPNA), Pamplona, Navarre, in 2011. Since then he has been working in the 'FASTER' research project at UPNA. He obtained a Master of Communications in 2012, held by the UPNA and he is currently pursuing the Ph.D degree in Telecommunication Engineering. His research interests include radio propagation, modeling of radio interference sources and mobile radio systems.

Leire AZPILICUETA received her Telecommunications Engineering Degree from the Public University of Navarre (UPNa), Pamplona, Spain, in 2009. In 2010 she worked in the R&D department of RFID Osés as radio engineer. In 2011, she obtained a Master of Communications held by the Public University of Navarre. She is currently pursuing the Ph.D. degree in telecommunication engineering. Her research interests are on radio propagation, mobile radio systems, ray tracing and channel modeling.

Juan Antonio NAZABAL was born in Pamplona, Spain, in 1977. He received his B.S. degree in Telecommunications Engineering from the Public University of Navarre (UPNA), Pamplona, Spain, in 2003. In 2010, he obtained a Master of Communications held by the Public University of Navarre. He is currently pursuing the Ph.D. degree in Telecommunication Engineering. His research interests are system integration, building automation and mobile radio systems.

Carlos FERNÁNDEZ-VALDIVIELSO received his Telecommunications Engineering Degree in 1998 and in 2003 his PhD in Communications, both from the Universidad Pública de Navarra, Navarra, Spain. In 1998 he co-founded Ingeniería Domótica, a company devoted to smart buildings and home automation systems. In 2005 he became an Associate Professor at UPNA. Since 2012 he is Director of SODENA, a venture capital company.

Jesús SORET received his Telecommunications Engineering Degree in 1998 and in 2003 his PhD in Communications, both from the Universidad de Valencia (UV), Spain. Since 2005 he is an Associate Professor at UV, working on wireless sensor systems.

Francisco FALCONE received his Telecommunications Engineering Degree in 1999 and his PhD in Communications in 2005, both from the Universidad Pública de Navarra, Navarra, Spain. From 1999 to 2000 he worked in Siemens-Italtel as a Microwave Engineer. From 2000 to 2008 he was a Radio Network Engineer in Telefónica Móviles. In 2009 he co-founded Tafco Metawireless, a spin-off company devoted to complex EM media. In parallel, he was an Assistant Professor at UPNA and since 2009, an Associate Professor at UPNA.